Modelling of transient wind turbine loads during pitch motion (paper and poster)

Sørensen, Niels N.; Aagaard Madsen, H.

Published in:
Proceedings (online)

Publication date:
2006

Document Version
Peer reviewed version

Modelling of transient wind turbine loads during pitch motion

Niels.N. Sørensen, Helge Aa. Madsen, Risø National Laboratory, DK-4000, Roskilde, Denmark, Ph. 45 46775053, nns@risoe.dk

Abstract
In connection with the design of wind turbines and their control algorithms, the transient loads, especially generated by time varying blade loads, are very important. In the Blade Element Momentum method, the most widespread tool in the wind turbine industry, the time constants necessary to describe these problems are not an inherent part of the model. In the present study two different approaches are used to determine these time constants, namely the EllipSys3D Navier-Stokes solver, and an actuator disc method. The time constants estimated by the actuator disc method is afterwards used in a standard BEM method and a BEM method coupled with a near wake method. The resulting transients are compared to measured values, for a step pitch change taken from the unique data set of the NREL/NASA Ames experiment, with good agreement for the case with low loading. Following this, a series of pitch steps corresponding to more realistic operational conditions are investigated.

Introduction
Dealing with transient aerodynamic loads for wind turbine these are typically handled at two levels, unsteady airfoil aerodynamics, and the so called dynamic inflow models. The first part covers the unsteady non-separated effects from shed vorticity [1,2] and the dynamic stall models, phenomena which both deals with relatively fast motion with a time scale in the order of the chord divided by the velocity seen by the airfoil. The second part of the dynamic loads, the dynamic inflow, or dynamic induction, is phenomena related to variations in the inflow velocity, structural vibrations and tip pitch changes. The time scales important for this are of size rotor radius divided by the free stream velocity. In the present paper the main focus is on the second part of these models namely the dynamic inflow models.
Dynamic inflow models have been developed early on in connection with helicopter aerodynamics for forward flight, see [3],[4]. It is important though to be aware that as stated in earlier work dealing with dynamic inflow, [5], that the wind turbine operational conditions are different from the conditions experienced in connection with helicopters. First of all, wind turbines are designed for power extraction at high induction factors ~1/3, while helicopters are designed for maximum thrust with minimum power consumption at low induction factors. As the dynamic inflow problem is closely related to the induction, and is most important for high induction factors, some of the assumptions used in connection with the helicopter related models may not be applicable for wind turbine aerodynamics.
Basically, the dynamic inflow models describe the effect that when the load changes, for example due to a change in blade pitch, this will not be instantaneously reflected in the induced velocity field, but gradually a new equilibrium will be established between the load on the blade, the rotor wake and the induced velocity at the rotor plane.
The direct consequence of the load overshoots experienced in connection with fast pitch changes, are of minor importance for the necessary structural strength of the turbine and the extreme loads. The main area of concern for these phenomena is the influence on the damping properties in connection with dynamic instabilities and vibrations. The importance of the values of the damping coefficients was investigated in [6], showing that neglecting the transient behavior will result in overestimating of the aerodynamic damping, that may result in unwanted vibrations in the real turbine.

When investigating problems related to dynamic inflow, one problem is to obtain accurate and detailed measurements. One source for this has been the Tjæreborg wind turbine experiment [7, 8, 9, 10, 11]. Even though these measurements have very good quality, they lack detailed information about the spanwise load distribution along the blade. In connection with the NREL/NASA Ames wind tunnel test [12, 13], detailed measurements were taken for a series of operational conditions [14] ranging from upwind axial operation, down wind operation, yaw operation and a series of step pitch operation that are interesting in connection with the present investigation.
In the current work, one series of step pitch changes taken from [15] are investigated using both a full 3D CFD code, and two versions of the BEM model, with the main focus of looking at the time constants for the settling of the loads. Following the comparison with measurements, a parametric study is performed to investigate the dynamic inflow effects for other operational conditions.

Code description/Method
The in-house flow solver EllipSys3D used in the present study for the CFD computations, is developed in co-operation between the Department of Mechanical Engineering at DTU and The Department of Wind Energy at Risø National Laboratory, see [16, 17 and 18]. The EllipSys3D code is a multi-block finite volume discretization of the incompressible Reynolds Averaged Navier-Stokes (RANS) equations in general curvilinear coordinates, and is second order accurate in both time and space. The code is parallelized with MPI for executions on distributed memory machines, using a non-overlapping domain decomposition technique. In the present work the turbulence in the boundary layer is modeled by the k-ω SST eddy viscosity model [19]. The rotation and pitch of the rotor is modeled using a moving mesh formulation in a fixed frame of reference. The moving mesh option has been

implemented in the EllipSys3D solver in a generalized way allowing arbitrary deformation of the computational mesh, following [20]. It has been used for doing unsteady simulations for several years both for stiff rotors in yaw and fully coupled aeroelastic computations [21, 22, 23, 24]. The mesh used in the present study has 5.2 million points and has previously been used in connection with yaw computations [21], where more details can be found.
Additionally, two engineering models are used in the present study; a Blade Element Momentum model (BEM model) and a BEM model coupled to a near-wake model (NW model).
The BEM model is well-known and is used in almost all aeroelastic models to compute the induction, [25]. Basically, the BEM model is a steady model and therefore a sub-model must be introduced to compute the unsteady induction caused by load changes on the rotor due to e.g. pitch changes or eigen-motion of the rotor or the blades. This sub-model must simulate the delay in changes of induction at the rotor disc when going from one loading on the disc to another loading. Such a load change will cause a change in trailed and shed vorticity from the rotor blades and the new state is first stationary when the whole wake system of the rotor corresponds completely to the new loading on the rotor. In the present implementation of the dynamic induction model a filter function is applied on the instantaneous computed induced axial velocity at the rotor disc. Both a 1st order and a 2nd filter have been tested. The filter is modeled using the indicial function technique. Besides the model for filtering the induced velocity it is necessary with a sub-model for computating the effect of the shed vorticity in order to model the complete influence of the vortex system in the wake properly. This is also done with an indicial function technique and follows the implementation in the Beddoes-Leishman dynamic stall model, [26].
The near wake model was originally developed by Beddoes, [27], for computation of high time resolution air loads on helicopter rotors, and is a way to include the radial dependency of the loads. Recently it has been implemented at Risø for use on wind turbine rotors, [28]. In short, the main idea with the model is to simulate the downwash from the first 90 degree of the trailed vortex system behind the individual blades with a simple, unsteady lifting line model. Again the indicial function technique is used to compute the downwash in the model. As the near wake model only computes the induction from the first part of the trailed vortex system, a model to compute the induction from the far wake is needed. In the present case a BEM model is used but where the loading in the form of the local thrust coefficient is scaled down with a constant which in the present case is 0.85. This constant was found correlating the load distribution in the combined NW model with the result of a standard BEM computation. It should be noted that no tip correction is used in the NW model as the trailed vortex system of the individual blades are modeled and forces the loading at the tip to approach zero. The same model for the shed vorticity as described above is also used in the NW model.
Actuator disc simulations with a uniform loading and with a step change from one thrust coefficient to another has been used as a basis for estimation of time constants to be used in both engineering models. For the NW model only one time constant is used as the NW model itself takes care of the initial fast decay, while the slower decay must be handled by the filtering of the induced velocities. Normally, the time constants are made dimensionless using the free stream velocity and the radius of the rotor. Another option used in the present work is to use the instantaneous velocity in the wake for the normalization

$$\tilde{t} = t\,\frac{V_\infty(1-1.5a)}{R}.$$

In both the BEM and the NW model, this is the approach used, and as will be seen later in the paper, this assures that the time constants reflects the slower development of the wake when high induction are present. The effect of changing the normalization can be seen in Figure 1, where the use of the actual wake velocity makes the curves collapse.

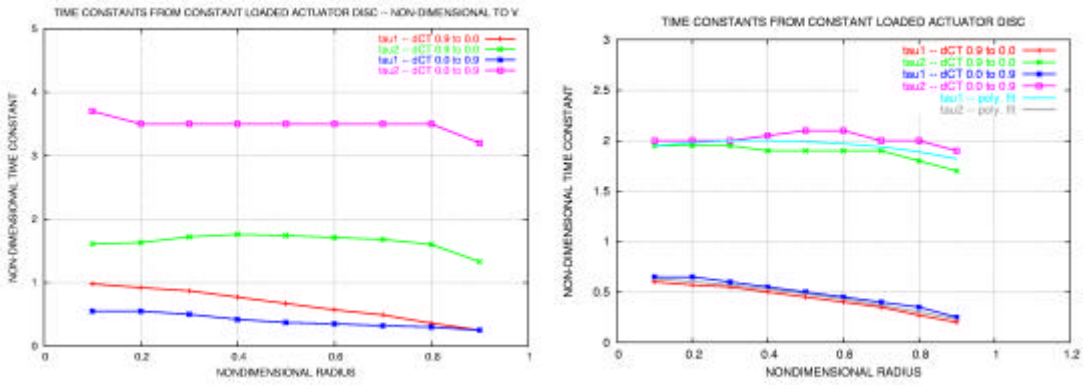

Figure 1: The dependency of the non-dimensionale time constant on the choice of normalization velocity used, left figure using the free stream velocity, right figure shows the use of the actual wake velocity.

In the present work, when analyzing the transient behavior of the dynamic inflow effects of both the experiment and the numerical simulations, the dynamic inflow effects are parameterized as a sum of two exponential decay functions,

as shown below. The sum of two exponential functions is used, instead of just a single one, as a compromise to allow us to capture both the fast decay initially and the more slow decay in the last stage of the development towards equilibrium.

$$c = (1-a)\exp(-(t-t_0)/t_1) + a\ \exp(-(t-t_0)/t_2)$$

Alternatively an expression where the time 'constant' is directly a function of time could be used. The normal forces, F_n, are normalized using the following expression:

$$\tilde{F}_n = \frac{F_n - F_\infty}{F_0 - F_\infty},$$

where F_8 is the value at equilibrium, and F_0 is the peak value before the actual decay sets in. Both the experimental as well as some of the computed results exhibit some high frequency oscillations, and the determination of the time constants are performed by visual inspection.

Experimental data

During the test of the UAE in the NASA Ames tunnel, a series of runs were dedicated to investigate dynamic inflow effects. These measurements were all performed for the upwind configuration with 0 degrees cone angle. The dynamic inflow tests for the NREL Phase-VI turbine all have relatively large pitch amplitude of either 16 or 18 degrees, which except for braking action is far from the pitch changes seen in normal wind turbine operation, where typical values around +/- 5 degrees pitch are used. Additionally, the pitch rate of 66 [degrees/s] of the UAE test is rather high compared to typical pitch rates for full scale turbines, where values of 5 [degrees/s] are typical. The wind speeds available in the experiment are 5, 8, 10 and 15 m/s. The dynamic induction effects are expected to be most pronounced at the lower wind speeds, and at large pitch amplitudes.

The data selected from the NREL Phase-VI experiment is a case with a tunnel speed of 5 [m/s], a minimum tip pitch of minus 6 degrees, and a maximum tip pitch of 10 degrees. The maximum pitch rate is 66 degrees/s, and the time delay between consecutive pitch changes are 15 seconds to allow the flow to settle between the pitch changes. The data has been processed and used previously in [29], and was kindly made available for the present study. The actual pitch movements are shown in Figure 2, which shows the acceleration and deceleration of the blades during the pitch movement at start and stop compared to the max pitch speed curve.

In the computations the actual pitch curves including acceleration and deceleration are used, since a direct use of just the linear curve from Figure 2 results in highly oscillatory blade loads at the start and stop of the movement.

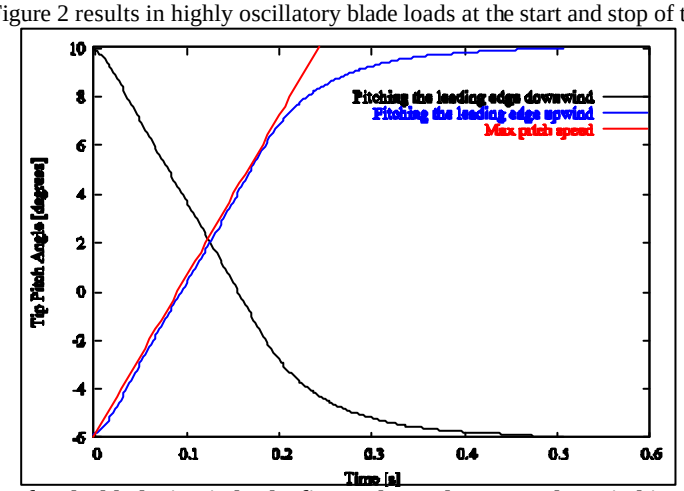

Figure 2: Time history for the blade tip pitch, the figure shows the curve when pitching from 10 to minus 6 degrees pitching the leading edge downwind, the curve when pitching from minus 6 to 10 degrees pitching the leading edge upwind, and the curve that are obtained for the minus 6 to 10 degrees step pitch using the specified pitch rate of 66 [deg/s].

Doing very large pitch steps, the change to the tunnel blockage may be an issue of concern especially at low wind speeds. In [30], the blockage is estimated for three different blade pitch angles, namely 0, 3 and 6 degrees. As seen in this reference an increasing blockage is found for decreasing pitch angle and for 5 m/s around 2 percent blockage is found for a tip pitch of 0 degrees. For the present step pitch change, the blade pitch angle has a minimum value of minus 6 degrees at 5 [m/s], and judging from the non-linear behavior reported in [30], the blockage may be nearly 4 to 5 percent for this tip pitch setting.

Results

In connection with the CFD computations, both time step investigations and mesh resolution investigations were performed. The time step investigations were performed on mesh level-2, a mesh with each second point removed,

for the following series of time-steps per revolution [833, 1666, 3333, 8333]. Looking at the shaft torque, the thrust, and distributions at five radial stations r/R= [0.30, 0.47, 0.63, 0.80, 0.95] of the pressure and chordwise skin friction, minimal difference was observed. Comparing computations for 833 time-steps per revolution for the level-2 grid and the finest grid level, small deviations in the sectional forces can be observed, but the influence on the time constants are very limited. As the level-1 computations, with 830 time-step per revolution takes approximately 4 hours/revolution on 20 CPU's, using the in house 240 CPU cluster of Dell PowerEdge 750 3.2 GHz Pentium 4 (32 bit) interconnected with D-Link 3324SR(I) Gigabit switches, and the level-2 mesh only takes approximately one eights of this time, most of the computations were performed with the level-2 mesh. In the CFD computations a delay time of 20 seconds were used instead of the 15 seconds used in the experiment, to allow a longer settling time for the flow. Based on this a step pitch change including both an upward and downward step, requires a minimum of 60 revolutions to be completed based on the 0.83 seconds per revolution used by the NREL Phase-VI turbine.

The computed shaft torque using the EllipSys CFD code is compared to the measured values in Figure 3. The overall agreement is reasonably good. For the 10 degrees tip pitch, where a negative shaft torque is observed, the CFD code predicts a slightly larger negative torque at the equilibrium state, while the overall transient behavior except for the lack of oscillation agrees reasonably well with the measured curve. For the minus 6 degrees tip pitch, where the turbine is heavily loaded, the shaft torque predicted by the CFD code is slightly low, and the decay is much slower than observed in the experiment. The difference in the decay rate may be connected to the extremely high axial induction in this situation, and the previously mentioned associated blockage effects. Concerning the high frequency oscillations seen in the measurements, these may be partly connected to torsion vibrations in the shaft, caused by the abrupt change in the shaft torque. As the model runs do not allow any structural deformations, these effects are not present in the computed results. Computed flapwise blade root moment using the engineering models and the experimental values are compared in the right side of Figure 3, showing excellent agreement, again the high frequency response seen in the experiments may be connected to structural vibrations of the turbine.

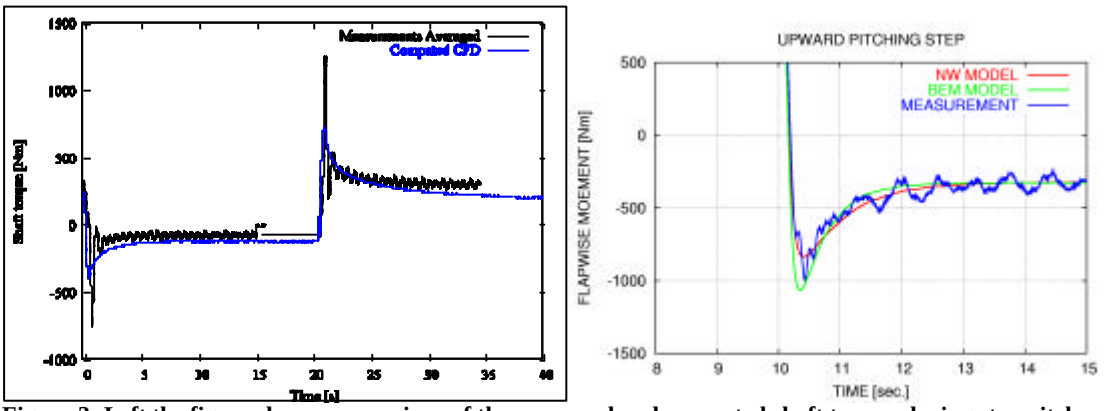

Figure 3: Left the figure shows comparison of the measured and computed shaft torque during step pitch changes, using the EllipSys3D code. At t=0 [s] the rotor is pitched from minus 6 to 10 degrees deloading the rotor, this is followed by a pitch step from minus 6 to 10 degrees initiated at approximately t=20 [s]. The right side of the figure shows comparison of the flapwise blade moment for the NW and the BEM model with the measurements, for a step from minus 6 to 10 degrees, deloading the rotor.

To illustrate the variation in axial induction for the two tip pitch angles, the variation of the axial velocity is computed along the flow direction for the five sections where the forces are measured in the experiment, see Figure 4. It is clear from this figure, that nearly no axial induction is seen for the 10 degrees tip pitch case, while an average axial induction of ~ 0.5 is seen for the minus 6 degrees case. For the minus 6 degree case, reversed flow is observed downstream in the tip region of the wake. The corresponding wake patterns behind the rotor are shown in Figure 5, where the tip and root vortices are visualized by an iso-surface of the absolute value of the vorticity, along with contours of vorticity in a horizontal slice. For the low load case, the 10 degrees tip pitch, the trailed vorticity is uniformly distributed along the blade span, while the vorticity is much more concentrated in the tip and root region for the high load case.

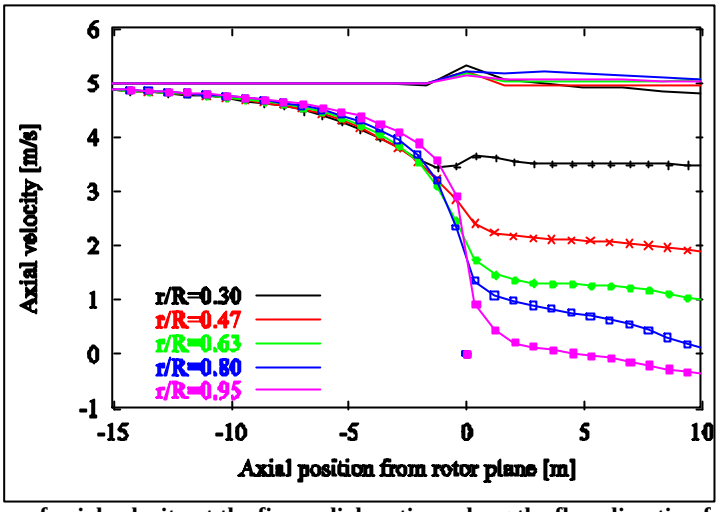

Figure 4: Distribution of axial velocity at the five radial sections along the flow direction from one and a half diameters upstream to one diameter downstream. The 10 degrees case (low load case) is shown with lines, while the minus 6 degrees case (high load case) is shown with lines and symbols.

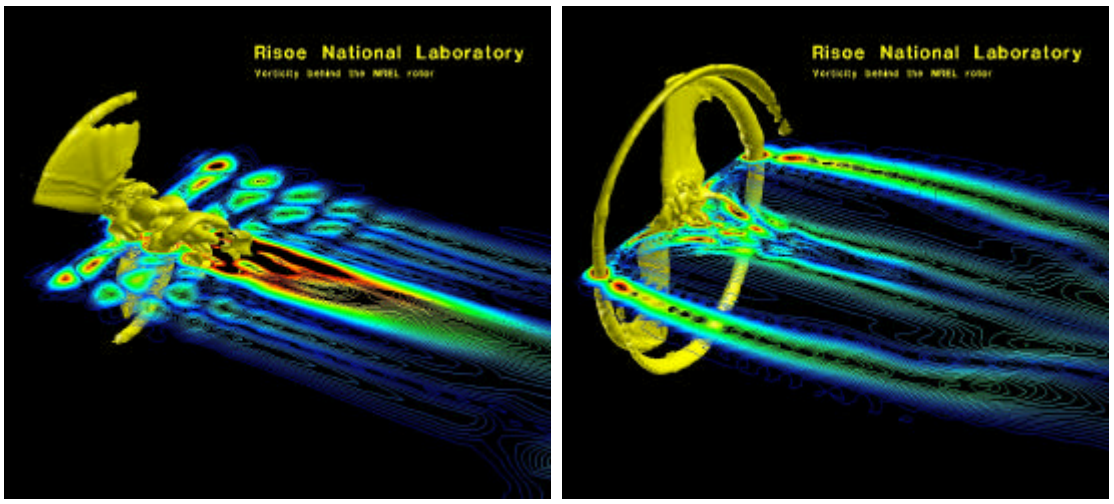

Figure 5 Wake patterns behind the rotor for the case with low loading left, 10 degrees, and high loading right, minus 6 degrees, showing the absolut value of the vorticity in a cut plane behind the rotor.

Estimating the two time constants for the exponential decay functions for the case where the rotor is de-loaded, based on the variation of the normal force coefficients along the blade span the values given in Table 1 can be found. Both the CFD, and the NW model reproduces the qualitative radial variation of the time constants from the root to the tip, while the BEM model shows very limited variation. For the measurements and the CFD and NW models, the radial dependency is mainly caused by the fast initial variation controlled by the t_2 constant. Even though there is good qualitative agreement for the CFD and NW models the actual values of the time constants shows some deviations. The decay functions corresponding to the time constants for the different models and the experiments are shown in Figure 6 to Figure 9.

Table 1: Time constants estimated when pitching from minus 6 to plus 10 degrees, changing the situation from a lightly to a highly loaded rotor.

	$t_{1\text{-min}}$ [s]	$t_{1\text{-max}}$ [s]	$t_{2\text{-min}}$ [s]	$t_{2\text{-max}}$ [s]
Measurements	0.9	1.2	0.3	0.9
CFD	1.3	1.7	0.2	0.8
BEM	1.3	1.5	0.5	0.5
NW	1.0	1.0	0.4	0.8

For the pitch step in the opposite direction, pitching from the lightly loaded 10 degrees to the highly loaded minus 6 degrees tip pitch situation, the observations are quite different, Figure 6 to Figure 9.Here both the experimental values

the CFD and the NW computations shows a very limited radial variation of the time constants over most of the rotor blade, with only the outermost sections deviating from the remaining sections. The NW model though indicates that the tip variation is fastest in contradiction with both measurements and CFD. The fact that there is a very limited agreement between the numerical values of the time constants may be closely related to the very high induction and the related tunnel effects in this situation, and the fact that no dynamic stall model is included in the BEM and NW models. Estimating the induction from Figure 4 and from the standard analytical expression relating thrust and induction, a value around a=0.5 is found from the CFD computations. Even though the induction in the experiment may be different from the computed value, all models reflects the fact that high induction results longer time constants for the slowest part of the dynamic inflow development. Comparing the time constants for the BEM and NW models for the upward and downward pitching step, it is clear that the use of the wake velocity instead of the free stream velocity results in an increased time constants for the case with high induction.

Table 2: Time constants estimated when pitching from 10 degrees to minus 6 degrees, changing the situation from a light to a highly loaded rotor.

	$t_{1\text{-min}}$ [s]	$t_{1\text{-max}}$ [s]	$t_{2\text{-min}}$ [s]	$t_{2\text{-max}}$ [s]
Measurements	2.5	2.5	0.3	0.3
CFD	4.9	4.9	0.6	0.6
BEM	2.0	2.2	0.2	0.8
NW	1.2	1.5	0.8	1.5

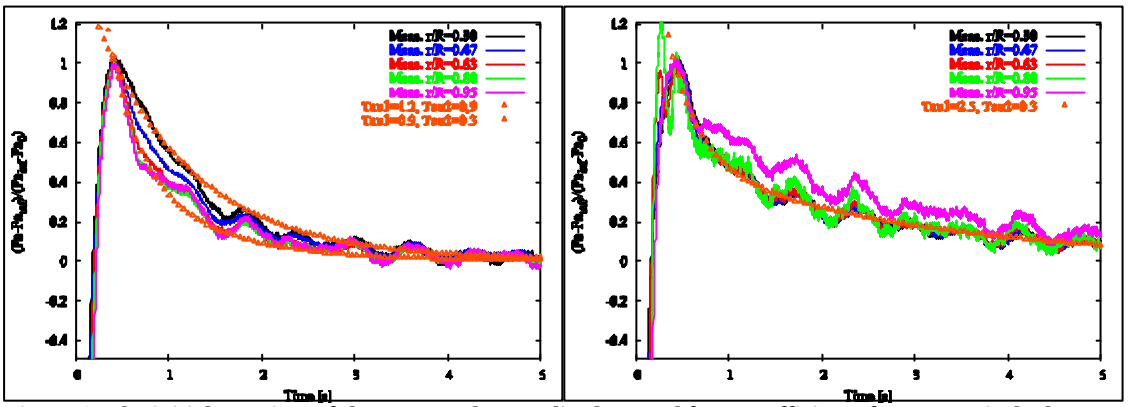

Figure 6: The initial transient of the measured normalized normal force coefficient after respectively de-loading the rotor by pitching to 10 degrees tip pitch right, and when loading the rotor by pitching to minus 6 degrees left.

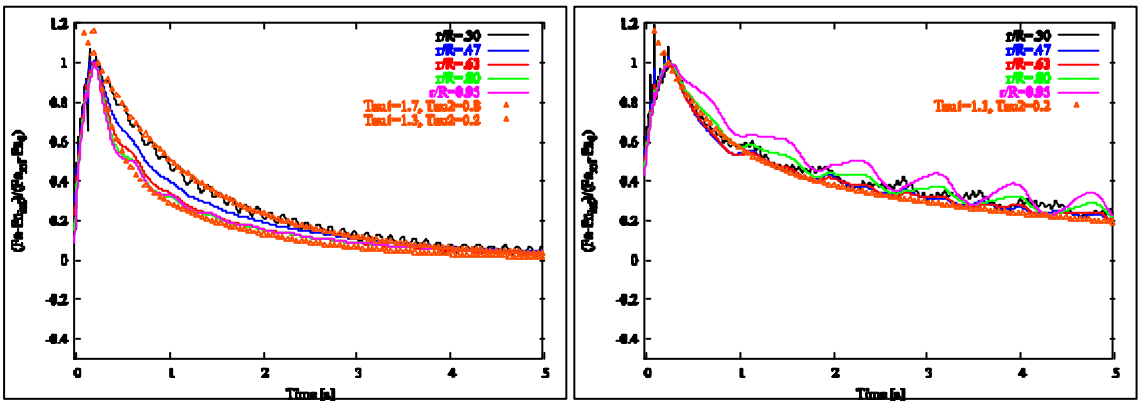

Figure 7: The initial transient of the computed normalized normal force coefficient using the CFD model after respectively de-loading the rotor by pitching to 10 degrees tip pitch right, and when loading the rotor by pitching to minus 6 degrees left.

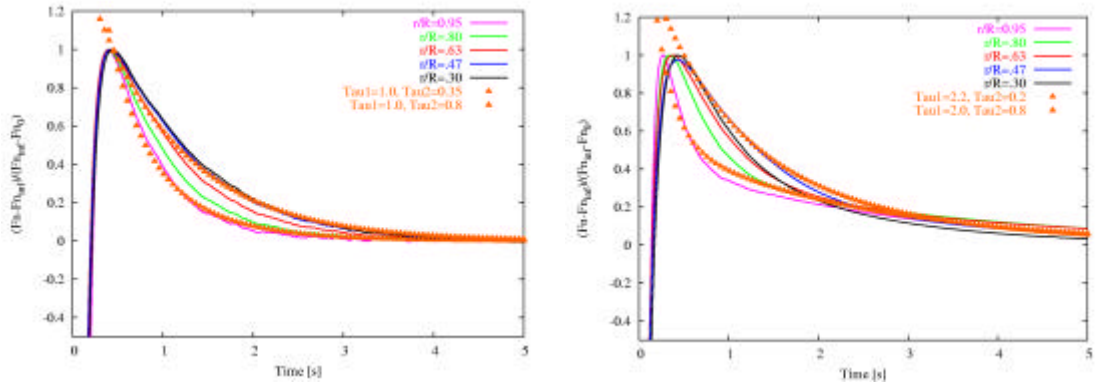

Figure 8: The initial transient of the computed normalized normal force coefficient using the BEM model after respectively de-loading the rotor by pitching to 10 degrees tip pitch right, and when loading the rotor by pitching to minus 6 degrees left.

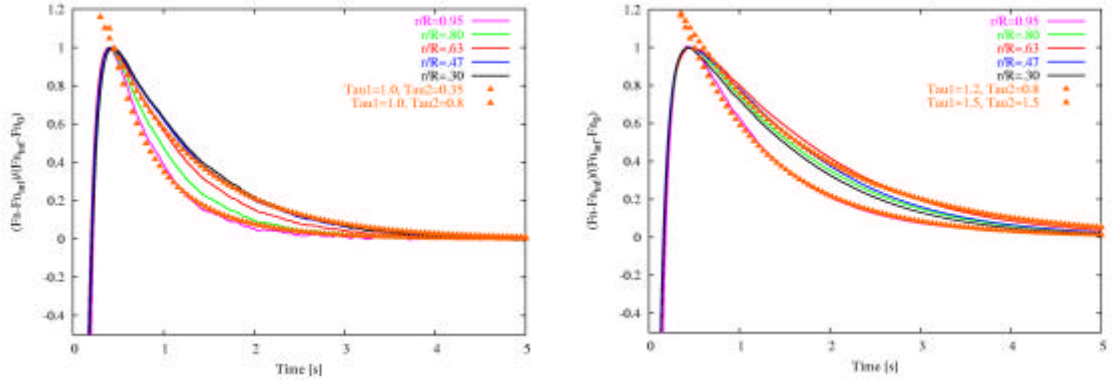

Figure 9: The initial transient of the computed normalized normal force coefficient using the NW model after respectively de-loading the rotor by pitching to 10 degrees tip pitch right, and when loading the rotor by pitching to minus 6 degrees left.

Following the comparison with the dynamic inflow test from the NREL experiment, a series of alternative pitch steps and wind speeds were investigated, all with smaller pitch amplitude more likely to be used in normal turbine operation, see Table 3. To estimate the induced velocity for the CFD computations the analytical expression $C_T=4a(1-a)$ is used. A plot of the two different ways of normalizing the time constants are shown in Figure 10, clearly showing a much more universal value of the time constant as function of C_T using the actual wake velocity.

The general picture from the different pitch step variations performed with the CFD code, indicates that for the typical pitch amplitude around 4 degrees, a very limited radial variation will be observed. Additionally, using a normalization based on the actual wake velocity, a limited variation is observed in both the slow and the fast time constant, with a value for the slow time constant between 1.5 to 2.0.

Table 3: Operational conditions, computed thrust, induction factor and time constants determined from the CFD computations doing different pitch steps and using different free stream velocities.

Free stream velocity [m/s]	Tip Pitch [degrees]		Thrust Coefficient		Induction factor after the step	Time constants [s]		Time constants normalized by wake velocity		Time constants normalized by free stream velocity	
	Initial	Final	Initial	Final	a	t_1	t_1	t_1	t_2	t_1	t_2
5	-6	10	1.06	0.04	-0.01	1.5	0.5	1.48	0.49	1.50	0.50
5	10	-6	-0.04	1.06	0.48	4.9	0.6	1.37	0.17	4.90	0.60
5	4	8	0.43	0.11	0.03	1.1	0.2	1.05	0.19	1.10	0.20
7	4	8	0.43	0.26	0.07	1.1	0.2	1.38	0.25	1.54	0.28
7	3	-1	0.47	0.63	0.20	1.4	0.3	1.37	0.29	1.96	0.42
7	10	2	0.17	0.52	0.15	1.2	0.2	1.30	0.22	1.68	0.28
7	2	10	0.52	0.17	0.04	1.2	0.2	1.58	0.26	1.68	0.28
7	5	1	0.39	0.55	0.16	1.2	0.3	1.28	0.32	1.68	0.42
7	-5	-1	0.75	0.63	0.20	2.2	0.3	2.15	0.29	3.08	0.42
7	-1	-5	0.63	0.75	0.25	2.0	0.3	1.75	0.26	2.80	0.42
10	4	8	0.36	0.28	0.08	1.1	0.2	1.94	0.35	2.20	0.40
10	8	4	0.28	0.36	0.10	1.1	0.2	1.87	0.34	2.20	0.40

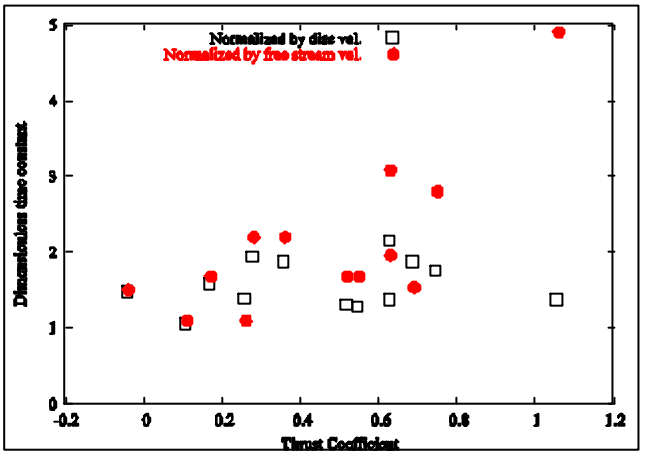

Figure 10: Non-dimensionalization of the time constants shown as function of the thrust coefficient of the rotor.

Conclusions

The use of the actual velocity in the wake instead of the free stream velocity in the BEM and NW model, allows the models to reflect the influence of the thrust coefficient on the transient behavior of the models. This corresponds to the observations in the NREL experiment. These findings are supported by the CFD results, showing a more universal time constant for the slowest part of the dynamic inflow process, using the wake velocity for normalization.
The parametric study of 4 and 8 degrees step pitch at 5, 7 and 10 [m/s] wind speeds using the CFD code EllipSys, revealed very limited radial dependency of the time constants for the dynamic inflow effects. Only in the case corresponding to the conditions from the NREL experiment changing the induction from nearly one to a value of zero, clear radial dependency can be seen.
The NREL NASA Ames data is a very useful data set, but especially for the dynamic inflow situations, care needs to be taken as the considerable changes in induction accompanying the large shift in thrust coefficient, may to some degree influence the conclusions especially for the high induction cases due to blockage effects.

Acknowledgements

This work was carried out under a contract, ENS-33031-0077, "Research program in applied aeroelasticity". The CFD computations were made possible by the use of the Risø 240 nodes MARY PC-cluster, and the computational resources of the Danish Centre for Scientific Computing at MEK/DTU in Lyngby.
A special thanks to J.G. Schepers, allowing us to use his processed version of the NREL/NASA Ames dynamic inflow data, originally processed for a similar study.

References

[1] Theodorsen, T. 1935. General Theory of Aerodynamic Instability and the Mechanism of Flutter, NACA Report 496.

[2] Wagner, H. Uber die Entstehung des dynamischen Auftriebes von Tragflugeln, Zeitschrift f¨ur Angewandte Mathematik und Mechanick, Vol. 5, No. 1, 1925.

[3] Bramwell ARS. Helicopter Dynamics. Edward Arnold (Publishers) Ltd, ISBN 0 7131 3353 8, 1976.

[4] Johnson W. Helicopter Theory. Princeton University Press, 1980.

[5] Schepers J.G. and Snel H. (ed.s'), Joint Investigations of Dynamic Inflow Effects and Implementation of an Engineering Method, ECN-C-94-107, Netherlands Energy Research Foundation ECN, 1995.

[6] Madsen, H.A. and Rasmussen F. A Near Wake Model for Trailing Vorticity Compared with the Blade Element Momentum Theory. Wind Energ. 2004; 7:325-341.

[7] Øye S.Tjæreborg wind turbine(Esbjerg) Fist dynamic inflow measurements. AFM Notat VK-189, Technical University of Denmark, 29 April. 1991.

[8] Øye S. Tjæreborg wind turbine (Esbjerg) 2. dynamic inflow measurement. AFM Notat VK-197, Technical University of Denmark, 11 September 1991.

[9] Øye S. Tjæreborg wind turbine (Esbjerg) 4. dynamic inflow measurement. AFM Notat VK-204, Technical University of Denmark, 25 Oktober 1991.

[10] Øye S. Tjæreborg Wind turbine (Esbjerg) Transient response measurements. AMF Notat VK-214, Technical Universithy of Denmark, 9 March 1992.

[11] Øye S. Tjæreborg wind turbine (Esbjerg) 6. dynamic inflow measurement. AFM Notat VK-234, Technical University of Denmark, 20 Oktober 1992.

[12] Fingersh L.J. et al " WIND TUNNEL TESTING OF NREL'S UNSTEADY AERODYNAMICS EXPERIMENT", ", AIAA-2001-0035 Paper, 39th Aerospace Sciences Meeting & Exhibit,2001, Reno.

[13] Simms, D., Schreck, S., Hand, M., Fingersh, L.J. NREL Unsteady Aerodynamics Experiment in the NASA-Ames Wind Tunnel: A Comparison of Predictions to Measurements. NREL/TP-500-29494. June 2001.

[14] Hand, M., Simms, D., Fingersh, L.J., Jager, D., and Larwood, S. Cotrell,J., and Schreck, S. Unsteady Aeorydnamics Experiment Phases VI: Wind tunnel Test Configurations and Available Data Campaigns. NREL/TP -500-29955, Nat. Ren. Energy Lab., Golden,CO, 2001.

[15] Hand, M., Simms, D., Fingersh, L.J., Jager, D., and Larwood, S. Cotrell,J., and Schreck, S. Unsteady Aeorydnamics Experiment Phases VI: Wind tunnel Test Configurations and Available Data Campaigns. NREL/TP -500-29955, Nat. Ren. Energy Lab., Golden,CO, 2001.

[16] Michelsen J.A., "Basis3D - a Platform for Development of Multiblock PDE Solvers" Technical Report AFM 92-05, Technical University of Denmark, 1992.

[17] Michelsen J.A., "Block structured Multigrid solution of 2D and 3D elliptic PDE's", Technical Report AFM 94-06, Technical University of Denmark, 1994.

[18] Sørensen N.N., "General Purpose Flow Solver Applied to Flow over Hills", Risø-R-827-(EN), Risø National Laboratory, Roskilde, Denmark, June 1995.

[19] Menter F.R., "Zonal Two Equation k-ω Turbulence Models for Aerodyanmic Flows". AIAA-paper-932906, 1993.

[20] Demirdzic, I., Peric, M. (1988): Space conservation law in finite volume calculations of fluid flow. Int. J. Numer. Methods Fluids, 8, 1037-1050.

[21] Sørensen, N.N., Michelsen, J.A. and Schreck, S., Application of CFD to wind Turbine Aerodynamics, 4th GRACM Concgress on Computational Mechanics, GRACM 2002, Patras, 27-29 June, 2002. Tsahalis, D.T. (ed.), (Greek Association of Computational Mechanics, [s.l.], 2002) 9 p.

[22] Madsen, H.A.; Sørensen, N.N.;Schreck, S.,YAW AERODYNAMICS ANALYZED WITH THREE CODES IN COMPARISON WITH EXPERIMENT, 22rd ASME Wind Energy Symposium, RENO NV(US), 6-9 Jan 2003.

[23] Bertagnolio, F.; Gaunaa, M.; Hansen, M.; Sørensen, N.N.; Rasmussen, F., Computation of aerodynamic damping for wind turbine applications. In: CD-Rom proceedings. 4. GRACM congress on computational mechanics, Patras (GR), 27-29 Jun 2002. Tsahalis, D.T. (ed.), (Greek Association of Computational Mechanics, [s.l.], 2002) 8 p.

[24] Bertagnolio, F.; Gaunaa, M.; Sørensen, N.N.; Hansen, M.; Rasmussen, F., Computation of Modal Aerodynamic Damping Using CFD, 22rd ASME Wind Energy Symposium, RENO NV(US), 6-9 Jan 2003.

[25] Galuert H. Aerodynamic Theory. Editor in-chief W.F. Durand. Vol. IV, Division L, p 179. Julius Springer, Berlin 1935.

[26] Leishman, J.G. Principles of Helocopter Aerodynamics. Cambridge University Press: Cambridge, 2000.

[27] Beddoes, T.S. A near wake dynamic model. Aerodynamics and Aeroacoustics National Specialist Meeting. Papers and discussion, 1987, pp 1-9.

[28] Madsen, H.A. and Rasmussen F. A near wake model for trailing vorticity compared with the blade element momentum theory. Wind Energy (2004) 7, 325-341.
[29] G. Scheppers IEA, Dynamic Inflow. IEA Joint Action Committee on aerodynamics, Annex XI and 20. Aero experts meeting, Pamplona (ES), 25-26 May 2005. Unpublished.
[30] Simms D., Schreck S., Hand M. and Fingersh L.J. NREL Unsteady Aerodynamics Experiment in the NASA-Ames Wind Tunnel: A Comparison of Predictions to Measurements. NREL/TP-500-29494. June 2001.